Electromechanical Modeling of the Low-Frequency Zigzag Micro-Energy Harvester

M. Amin Karami[1,*] and Daniel J. Inman[2]

[1]Department of Engineering Science and Mechanics, Virginia Tech, Blacksburg, VA 24061, USA

[2]Center for Intelligent Material Systems and Structures, Department of Mechanical Engineering, Virginia Tech, Blacksburg, VA 24061, USA

ABSTRACT: An analytical electromechanical model is proposed to predict the deflection, voltage, and the power output of a proposed low-frequency micro-harvesting structure. The high natural frequencies of the existing designs of micro-scale vibrational energy harvesters are serious drawbacks. A zigzag design is proposed to overcome this limitation. First, the natural frequencies and the mode shapes of the zigzag structure are calculated. The piezoelectric direct and reverse effect equations, together with the electrical equations, are used to relate the voltage output of the structure to the base vibrations magnitude and frequency. The closed-form solution of the continuous electromechanical vibrations gives the power output as a function of base acceleration spectrum. The usefulness of the design is proved by the significant increase of the power output from the same base accelerations, providing a method of designing a micro-scale harvester with low natural frequency. The optimal mechanical and electrical conditions for power generation are investigated through the case studies.

Key Words: energy harvesting, MEMS, low frequency, electromechanical modeling, piezoelectric.

NOMENCLATURE

b	the width of the lateral beams
GJ	torsional stiffness
h_p	thickness of the Piezo layer
h_s	thickness of the substructure
j	the unit imaginary number, $\sqrt{-1}$
$k = GJ/EI_x$	stiffness parameter
l	the length of each of the lateral beams
L	the left transformation matrix
M_t	tip mass
m_l	link mass
n	the total number of members
P_i	state of the ith switch
R	the right transformation matrix
$w_b(t)$	base vertical motion
$w_i(x, t)$	out-of-plane deformation of the ith beam
x_{end}	the x-coordinate of the free end
x^*	the x-coordinate of the connection of two lateral beams
Y_s	Young's modulus of substructure
Y_p	Young's modulus of piezoelectric layer
YI	bending stiffness
α	coupling figure of merit
$\beta_i(x)$	twist angle of the ith beam
κ_m	backward coupling coefficient
ρ_p	density of the piezoelectric material
ρ_s	density of the substructure material
ρA	mass per unit length
ψ_m	current generation coupling coefficient

*Author to whom correspondence should be addressed.
E-mail: karami@vt.edu
Figures 2–10 appear in color online: http://jim.sagepub.com

INTRODUCTION

The advances in low-power micro-electronics, micro-scale sensors, and smart actuators have paved the way to independent remote sensing nodes. It is now almost possible to have sensor packs spread on bridges to regularly do the structural health monitoring and to send the data wirelessly to the base. One component still needing improvement is the energy source needed to power the sensors and circuits. The traditional power sources, which are still widely used, are batteries. The necessity to change the batteries requires scheduled access to the devices, limiting their placement and increasing cost. The need of a self-sustained energy source has motivated many researchers in the recent years (Beeby et al., 2006; Anton and Sodano, 2007; Arnold, 2007; Priya, 2007; Cook-Chennault et al., 2008; Priya and Inman, 2008), who have considered

1045-389X/11/03 0271–12 $10.00/0 DOI: 10.1177/1045389X11398164

solar power, thermal gradients, and ambient vibrations for generating electrical energy. The devices which convert ambient vibrations kinetic energy to electrical power are mostly either electrostatic, electromagnetic, electrostricitve, or piezoelectric. We focus on the conversion of vibrational energy available in the environment in the form of transient oscillations to electricity using piezoelectric devices. Another goal is to have the energy-harvesting device as small as sensors and circuitry. Now that the micro-electromechanical systems (MEMS) sensors are being used, it is desired to design a harvesting device also in the micro-scale.

One of the main obstacles in the path to MEMS energy harvesting is the high resonant frequency of the micro-devices. The frequencies of typical ambient vibrations are from 1 to 100 Hz. The linear vibrational energy harvesters are highly sensitive to the frequency of the excitation. The power harvested at resonance frequency of the device is orders of magnitude larger than the power harvested off resonance. The natural frequency of the harvesters should, therefore, be less than 100 Hz. This has proven to be a major challenge in the development of MEMS harvesters. Many designs reported in the literature have thickness-to-length ratio of large-scale structures. This caused the corresponding natural frequencies to fall in the range of kHz (Lu et al., 2004; Jeon et al., 2005; Kuehne et al., 2008; Zheng and Xu, 2008). In reality, to have a structure which is strong enough to sustain the vibrations, the thickness has to be proportional to its length squared. This means that the thickness-to-length ratio of MEMS structures has to be way less than that ratio of their macro-scale counter parts. By choosing a thickness-to-length ratio of 1/100, Fang et al. (2006) were able to achieve 600-Hz natural frequency. The trend was followed by Shen et al. (2008) and Liu et al. (2008) and natural frequencies of about 460 and 100 Hz were achieved. The natural frequency has to be lowered further to match the ambient excitations; however, the cantilever beam design is too simple to facilitate lowering the frequency.

The authors proposed using the zigzag design (Figure 1) for MEMS vibrational energy harvesters (Karami and Inman, 2011). They analytically studied and experimentally verified the natural frequencies and the mode shapes of the meandering structure and showed that a harvester with the proper natural frequency can be achieved by utilizing the zigzag design. It was shown that not only a zigzag structure can have a significantly lower natural frequency compared to a cantilever beam of the same dimensions, but also this reduction of frequency is achieved without sacrificing the strength of the structure.

Spiral structures (Hu et al., 2007; Karami et al., 2010) have also been used to lower the natural frequency of the harvester. The main problem hindering the use of spiral geometry for harvesting application is the fact that the out-of-plane vibrations of the spirals are dominantly torsional (Karami et al., 2010). This requires complicated electrode configuration to be able to harness the generated energy.

This article continues by presenting details of the zigzag design followed by analysis of the coupled bending–torsion vibrations of the structure. Solving the free vibrations problem gives the natural frequencies and mode shapes of the structure. The response of the structure to the base vibrations is next analyzed and the piezoelectric direct and reverse effects are considered. The transfer functions between the base accelerations and the voltage and power outputs are calculated. Also, the tip deflection transfer function is derived with consideration of the backward coupling. The following are discussed: how the use of the zigzag design increases the power output, how the strength of zigzag structure is related to the number of members, and what are the optimal electrical and mechanical conditions required for power production.

ENERGY-HARVESTING DEVICE

The proposed MEMS energy harvester has a zigzag shape and is depicted in Figure 1. The base excitations make the structure vibrate in and out of the main plane. The structure is clamped at one end and supports a tip mass at its other end, forming a cantilever structure. It is modeled as a collection of straight beams, with rectangular cross-sections, placed next to each other on the main plane. Each beam is connected to its neighbor beams at its ends by the link portions. Each of the beams can bend out of the main plane and twist.

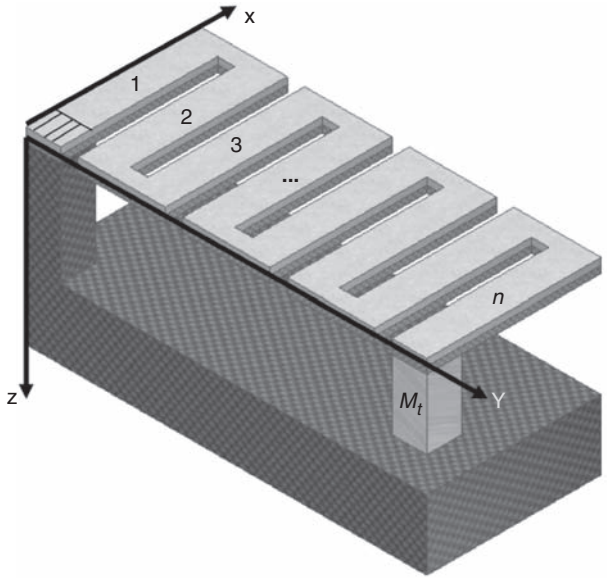

Figure 1. *The zigzag energy-harvesting structure.*

Since the links are short, we model them as rigid connections. We do, however, take their mass into consideration. The beams are composed of two layers. The bottom layer is the substrate layer made out of silicon for example. The top layer is the piezoelectric material. The piezoelectric layer is sandwiched between two metal electrode layers on its top and bottom surfaces. Due to the electrode configuration, the torsion of the individual beams does not generate any voltage across the electrodes and the harvested energy only attributes to the bending in the structure.

GOVERNING MECHANICAL EQUATIONS

The structure vibrates due to the bending and torsion of the individual beams. Each of the beams can bend, resulting in the deflection of that member and change in start position of the next beams. The members can also twist. The torsion of each of the beams does not affect the elevation of the points on that member, but will lower or raise the next beam. The amount of elevation (or demotion) is equal to the twist angle of the member times the distance between the two consequent beams.

The deformation of the lateral beams can be quantified with their twist angle, $\beta_i(x,t)$, and out-of-plane displacement, $w_i(x,t)$. The index i identifies each lateral beam. Both β_i and w_i are time dependent and vary along the beam and therefore are functions of x and t (Figure 2).

The piezoelectric constitutive equations relate strain and electric displacement field to the stress and the electric field. For bending vibrations of piezoelectric bi-layered beams poled in the thickness direction, the constitutive equations simplify to (Leo, 2007):

$$T_1 = Y_p(S_1 - d_{31}E_3) \tag{1a}$$

$$D_3 = -d_{31}Y_pS_1 - \varepsilon_{33}^s E_3 \tag{1b}$$

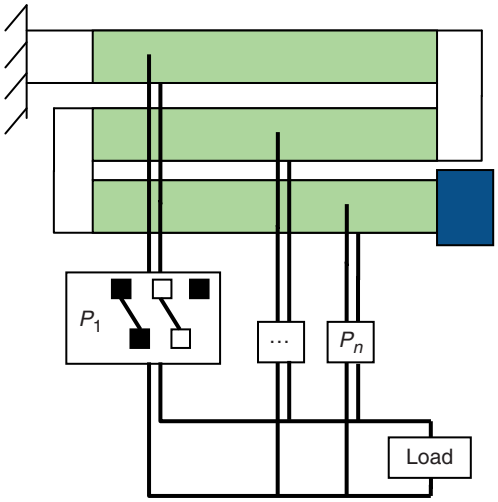

Figure 2. *Electrical connections, top view.*

In the above equations, T_1 represents normal stress along x-axis, S_1 the normal strain in the same direction, Y_p the Young's modulus of piezo layer, d_{31} the piezoelectric coupling coefficient, E_3 the electric field across the thickness of the piezo layer, D_3 the electric displacement along the thickness, and ε_{33}^s the permittivity at constant stress.

The constitutive equations can be used in the Euler–Bernoulli model of beams to give the following equations for bending vibrations of any of the beams (Erturk and Inman, 2008):

$$YI\frac{\partial^4 w_{rel}(x,t)}{\partial x^4} + \rho A\frac{\partial^2 w_{rel}(x,t)}{\partial t^2} = -\alpha v(t)\left[\frac{d\delta(x)}{dx} - \frac{d\delta(x-L)}{dx}\right] - \frac{[\rho A + M_t\delta(x - x_{end}, i-n)]d^2w_b(t)}{dt^2} \tag{2}$$

The coupling figure of merit α is equal to:

$$\alpha = -\frac{Y_p d_{31} b}{2h_p}\left(h_c^2 - h_b^2\right) \tag{3}$$

The equivalent bending stiffness of the composite beam, YI, is given below

$$YI = b\left[\frac{Y_s\left(h_b^3 - h_a^3\right) + Y_p\left(h_c^3 - h_p^3\right)}{3}\right]$$

ρA is mass per unit length of the beam and equals:

$$\rho A = b(\rho_s h_s + \rho_p h_p)$$

At first, the free vibration solution is calculated. The response of the electromechanically coupled structure to base vibrations will later be expressed in terms of free vibration solutions. Setting the left side of Equation (2) to zero results:

$$c^2\frac{\partial^4 w_i}{\partial x^4} + \frac{\partial^2 w_i}{\partial t^2} = 0,\ c = \sqrt{\frac{YI}{\rho A}} \tag{4}$$

A standard separation of variable solution is substituted next:

$$w_i(x,t) = W_i(x)T(t) \Rightarrow c^2\frac{w_i^{(4)}}{w_i} + \frac{\ddot{T}}{T} = 0 \tag{5}$$

$$-c^2\frac{w_i^{(4)}}{w_i} = \frac{\ddot{T}}{T} = constant = -\omega_n^2 \tag{6}$$

$$W_i^{(4)} + \frac{\omega_n^2}{c^2}W_i = 0,\ W_i = A_i e^{s_i x},\ \Rightarrow s_i^4 + \frac{\omega_n^2}{c^2} = 0$$

$$s_{ij} = \pm\sqrt{\frac{\omega_n}{c}}, \pm i\sqrt{\frac{\omega_n}{c}}, j = 1, 2, \ldots, 4 \tag{7}$$

$$W_i(x) = \sum_{j=1}^{4} A_{ij}\ e^{s_{ij}x} \tag{8}$$

The torsional equation of motion for the same beam is:

$$GJ\frac{\partial^2\beta_i}{\partial x^2} - I_p\frac{\partial^2\beta_i}{\partial t^2} = 0$$

where GJ is the equivalent torsional rigidity of the thin composite beam (Booker and Kitipornchai, 1971; Blevins, 1979) and is equal to

$$GJ = 3\frac{\frac{4\left(G_p h_p^3 + G_s h_s^3\right)}{3} - \frac{\left(G_p h_p^2 - G_s h_s^2\right)^2}{G_p h_p + G_s h_s}}{\left(h_p + h_s\right)^3} \times \frac{\left(h_s + h_p\right)^3 b^3}{3\left(b^2 + \left(h_s + h_p\right)^2\right)}$$

I_p is the mass axial moment of inertia of the beam per unit length about the axis of torsion and is approximated with

$$I_p \approx \frac{\rho_p}{12} b h_p\left(b^2 + h_p^2 + 3h_s^2\right) + \frac{\rho_s}{12} b h_s\left(b^2 + 3h_p^2 + h_s^2\right)$$

or

$$g^2\frac{\partial^2\beta_i}{\partial x^2} = \frac{\partial^2\beta_i}{\partial t^2},\ g = \sqrt{\frac{GJ}{I_p}} \tag{9}$$

The torsional vibrations of the structure are solely governed by mechanical properties, i.e. there is no electromechanical coupling in torsional vibrations. The torsional coupling coefficient is d_{15}, which means that the generated electric field from torsional vibrations is in the y direction. Since there are no electrodes on the vertical sides, there will be no current and the structure acts purely mechanically.

A separation of variables solution of the torsional equation is:

$$\beta_i(x,t) = B_i(x)T(t) \Rightarrow g^2\frac{B_i''}{B_i} = \frac{\ddot{T}}{T} = constant = -\omega_n^2$$

$$B_i'' + \left(\frac{\omega_n}{g}\right)^2 B_i = 0, \quad B_i = A_i e^{s_i x} \Rightarrow s_i^2 + \left(\frac{\omega_n}{g}\right)^2 = 0$$

$$s_{ij} = \pm i\frac{\omega_n}{g}, j = 5, 6 \tag{10}$$

$$B_i(x) = \sum_{j=5}^{6} A_{ij} e^{s_{ij}x} \tag{11}$$

In the next section, using Equations (8) and (11) and considering equilibrium and continuity conditions and the boundary conditions, we derive the natural frequencies and the mode shapes.

FREE VIBRATION MODE SHAPES

Each set of A_{ij} and S_{ij} corresponds to a certain resonance frequency. In order to calculate the mode shapes of the structure, we should find the exponents S_{ij} and the coefficients A_{ij} which result in non-trivial solutions in agreement with boundary conditions. The exponents are functions of the scalars ω_n (Equations (7) and (10)). It has been shown (Karami and Inman, 2011) that valid values of ω_n and A_{ij} correspond to non-trivial solutions of:

$$\begin{bmatrix} BC0_{3\times6} \\ BCe_{3\times6}\left[R_n^{-1}L_{n-1}R_{n-1}^{-1}\ L_{n-2}\ldots R_2^{-1}\ L_1\right]_{6\times6} \end{bmatrix}_{6\times6} \times \begin{bmatrix} A_{11} \\ \vdots \\ A_{16} \end{bmatrix} = 0_{6\times1} \tag{12}$$

where $\boldsymbol{BC0}$, $\boldsymbol{BCe}$, $\boldsymbol{R_i}$, and $\boldsymbol{L_i}$ are defined below:

$$[BC0]_{3\times6} = \begin{bmatrix} 1 & 1 & 1 & 1 & 0 & 0 \\ S_{11} & S_{12} & S_{13} & S_{14} & 0 & 0 \\ 0 & 0 & 0 & 0 & 1 & 1 \end{bmatrix} \tag{13}$$

$$[BCe]_{3\times6} = \begin{bmatrix} s_{n1}^2 e^{s_{n1}x_{end}} & s_{n2}^2 e^{s_{n2}x_{end}} & s_{n3}^2 e^{s_{n3}x_{end}} & s_{n4}^4 e^{s_{n4}x_{end}} & 0 & 0 \\ YIs_{n1}^3 e^{s_{n1}x_{end}} - M_t\omega_n^2 & YIs_{n2}^3 e^{s_{n2}x_{end}} - M_t\omega_n^2 & YIs_{n3}^3 e^{s_{n3}x_{end}} - M_t\omega_n^2 & YIs_{n4}^4 e^{s_{n4}x_{end}} - M_t\omega_n^2 & 0 & 0 \\ 0 & 0 & 0 & 0 & s_{n5}e^{s_{n5}x_{end}} & s_{n6}e^{s_{n6}x_{end}} \end{bmatrix} \tag{14}$$

$$L_{i-1}=\begin{bmatrix} e^{s_{(i-1)1}x^*} & e^{s_{(i-1)2}x^*} & e^{s_{(i-1)3}x^*} & e^{s_{(i-1)4}x^*} & d\,e^{s_{(i-1)5}x^*} & d\,e^{s_{(i-1)6}x^*} \\ s_{(i-1)1}e^{s_{(i-1)1}x^*} & s_{(i-1)2}e^{s_{(i-1)2}x^*} & s_{(i-1)3}e^{s_{(i-1)3}x^*} & s_{(i-1)4}e^{s_{(i-1)4}x^*} & 0 & 0 \\ 0 & 0 & 0 & 0 & e^{s_{(i-1)5}x^*} & e^{s_{(i-1)6}x^*} \\ -s^2_{(i-1)1}e^{s_{(i-1)1}x^*} & -s^2_{(i-1)2}e^{s_{(i-1)2}x^*} & -s^2_{(i-1)3}e^{s_{(i-1)3}x^*} & -s^2_{(i-1)4}e^{s_{(i-1)4}x^*} & 0 & 0 \\ -s^3_{(i-1)1}e^{s_{(i-1)1}x^*} & -s^3_{(i-1)2}e^{s_{(i-1)2}x^*} & -s^3_{(i-1)3}e^{s_{(i-1)3}x^*} & -s^3_{(i-1)4}e^{s_{(i-1)4}x^*} & 0 & 0 \\ 0 & 0 & 0 & 0 & GJ_{S(i-1)5}e^{s_{(i-1)5}x^*} & GJ_{S(i-1)6}e^{s_{(i-1)6}x^*} \end{bmatrix} \tag{15}$$

$$R_i=\begin{bmatrix} e^{s_{i1}x^*} & e^{s_{i2}x^*} & e^{s_{i3}x^*} & e^{s_{i4}x^*} & 0 & 0 \\ s_{i1}e^{s_{i1}x^*} & s_{i2}e^{s_{i2}x^*} & s_{i2}e^{s_{i2}x^*} & s_{i4}e^{s_{i4}x^*} & 0 & 0 \\ 0 & 0 & 0 & 0 & e^{S_{i5}x^*} & e^{S_{i6}x^*} \\ s^2_{i1}e^{s_{i1}x^*} & s^2_{i2}e^{s_{i2}x^*} & s^2_{i3}e^{s_{i3}x^*} & s^2_{i4}e^{s_{i4}x^*} & 0 & 0 \\ \left(\pm\frac{m_l\omega^2}{YI}+S^3_{i1}\right)e^{s_{i1}x^*} & \left(\pm\frac{m_l\omega^2}{YI}+S^3_{i2}\right)e^{s_{i2}x^*} & \left(\pm\frac{m_l\omega^2}{YI}+S^3_{i3}\right)e^{s_{i3}x^*} & \left(\pm\frac{m_l\omega^2}{YI}+S^3_{i4}\right)e^{s_{i4}x^*} & 0 & 0 \\ dYIs^3_{i1}e^{s_{i1}x^*} & dYIs^3_{i2}e^{s_{i2}x^*} & dYIs^3_{i3}e^{s_{i3}x^*} & dYIs^3_{i4}e^{s_{i4}x^*} & GJs_{i5}e^{s_{i5}x^*} & GJs_{i6}e^{s_{i6}x^*} \end{bmatrix} \tag{16}$$

The natural frequencies ω_n make the coefficients matrix of Equation (12) singular. Correspondingly, the first six coefficients A_{11} to A_{16} are derived. The rest of the coefficients are calculated from:

$$\begin{bmatrix} A_{i1} \\ \vdots \\ A_{i6} \end{bmatrix} = \mathbf{R_i^{-1}L_{i-1}} \begin{bmatrix} A_{(i-1)1} \\ \vdots \\ A_{(i-1)6} \end{bmatrix} \tag{17}$$

From this point on, we focus on a specific situation which the material and dimensions of all the members are identical. Equations (7) and (10) imply that the exponents of all the beams are identical as well and one can therefore drop the index distinguishing the member number:

$$s_j = \pm\sqrt{\frac{\omega_n}{c}},\ \pm i\sqrt{\frac{\omega_n}{c}},\ \pm\frac{i\omega_n}{g}\ j=1,\ldots,6 \tag{18}$$

The calculated coefficients give the mode shapes of the structure. The mth mode shape of the ith lateral beam is:

$$W_{mi}(x)=\sum_{j=1}^{4}A_{mij}e^{s_jx},\ B_{mi}(x)=\sum_{j=5}^{6}A_{mij}e^{s_jx} \tag{19}$$

Before proceeding to expressing the general solution in terms of the calculated mode shapes, we should first mass normalize them. Here, we neglect the rotational kinetic energy of the structure compared to its translational kinetic energy. The coefficients of mass normalized mode shapes are calculated as:

$$\begin{aligned} A_{mij} &= \frac{\widetilde{A_{mij}}}{\sqrt{M_m}}, \\ M_m &= \rho A\sum_{i=1}^{n}\int_0^L W^2_{mi}\mathrm{d}x + M_t W^2_{mn}(x_{end}) \\ &= \rho A\sum_{i=1}^{n}\sum_{j=1}^{4}\sum_{k=1}^{4}\frac{\widetilde{A_{mij}}\widetilde{A_{mik}}}{s_j+s_k}\left(e^{(s_j+s_k)L}-1\right) \\ &\quad + M_t\sum_{j=1}^{4}\sum_{k=1}^{4}\widetilde{A_{mnj}}\widetilde{A_{mnk}}e^{(s_j+s_k)x_{end}} \end{aligned} \tag{20}$$

where $\widetilde{A_{ij}}$ are the non-mass-normalized coefficients which result in the modal mass M_m.

ELECTROMECHANICAL MODEL

The members of the structure are electrically connected in parallel configuration, as depicted in Figure 2. The switches depicted in Figure 2 (small boxes) can be used to reverse the polarity of the generated voltage (or current). They determine whether the voltage across each member is equal to the voltage across the load or is its negative. Correspondingly, the switches also identify whether the current going into each member should be added to or subtracted from the current in other members to give the total current passing through the load.

Writing the vertical displacement function, w_{rel}, in the modal form and modifying Equation (2) to consider the switches role, we get:

$$\begin{aligned} &YI\sum\nolimits_{q=1}^{\infty}T_q(t)W^{(4)}_{qi} + \rho A\sum\nolimits_{q=1}^{\infty}\ddot{T}_qW_{qi} \\ &\quad = -\alpha P_i v(t)\left[\frac{\mathrm{d}\delta(x)}{\mathrm{d}x}-\frac{\mathrm{d}\delta(x-L)}{\mathrm{d}x}\right] \\ &\qquad -[\rho A + M_t\delta(x-x_{end},i-n)]\ddot{W}_b \end{aligned} \tag{21}$$

The state of the ith switch is P_i and either 1 or -1. Next, we multiply Equation (21) by W_{mi} and integrate

both sides from 0 to l. The orthogonality of the mode shapes results in:

$$YIT_m \int_0^l W_{mi} W_{mi}^{(4)} \mathrm{d}x + \rho A \ddot{T}_m \int_0^l W_{mi} W_{mi} \mathrm{d}x = -\alpha P_i v(t)\left[-W_{mi}'(0) + W_{mi}'(L)\right] - \left[\rho A \int_0^l W_{mi} \mathrm{d}x + M_t W_{mn}(x_{end})\right] \ddot{W}_b \mathrm{d}x \quad (22)$$

We can substitute for $W_{mi}^{(4)}$ and $\ddot{T}_m$ from Equation (5). Since the mode shapes are mass normalized, summation of the above equation over all the members gives:

$$\ddot{T}_m + \omega_m^2 T_m = -\kappa_m v(t) - \gamma_m \ddot{w}_b(t) \quad (23)$$

Equation (23) is the first of the two key governing differential equations in which:

$$\kappa_m = \alpha \sum_{i=1}^{n} P_i \left[W_{mi}'(l) - W_{mi}'(0)\right] = \alpha \sum_{i=1}^{n} P_i \sum_{j=1}^{4} A_{mij} s_j \left(e^{s_j l} - 1\right) \quad (24)$$

$$\gamma_m = \rho A \sum_{i=1}^{n} \int_0^l W_{mi} \mathrm{d}x + M_t W_{mn}(x_{end}) = \sum_{i=1}^{n} \sum_{j=1}^{4} \frac{A_{mij}}{s_j} \left(e^{s_j l} - 1\right) + M_t W_{mn}(x_{end}) \quad (25)$$

We can write Equation (23) in frequency domain by taking the Fourier transform of both sides:

$$\left(\omega_m^2 - \omega^2\right) \eta_m(\omega) = -\kappa_m V(\omega) + \gamma_m a(\omega) \quad (26)$$

In above $\eta_m(\omega)$, $V(\omega)$, and $a(\omega)$ are Fourier transforms of $T_m(t)$, $v(t)$, and $\ddot{w}_b(t)$, respectively. So far, the reverse piezoelectric effect has been modeled. We should now derive an expression for $v(t)$ as a function of deflection so that we have two equations for our two unknowns, $T_m(t)$ and $v(t)$.

Using Equation (1b), the current passing though each member is calculated (Erturk and Inman, 2008):

$$i_i(t) = -d_{31} Y_p h_{pc} b \frac{\mathrm{d}}{\mathrm{d}t} \left(\int_0^l \frac{\partial^2 w_{rel}}{\partial x^2} \mathrm{d}x \right) - \frac{\varepsilon_{33}^s b l P_i}{h_p} \dot{v}(t) \quad (27)$$

Writing the above equation in modal form gives:

$$i_i(t) = -d_{31} Y_p h_{pc} b \sum_{m=1}^{\infty} \left\{ \dot{T}_m(t) \left[W_{mi}'(l) - W_{mi}'(0) \right] \right\} - \frac{\varepsilon_{33}^s b l P_i}{h_p} \dot{v}(t) \quad (28)$$

We then take the Fourier transform of both sides:

$$I_i(\omega) = -j\omega d_{31} Y_p h_{pc} b \sum_{m=1}^{\infty} \left\{ \eta_m(\omega) \left[W_m'(l) - W_m'(0) \right] \right\} - j\omega \frac{\varepsilon_{33}^s b l P_i}{h_p} V(\omega) \quad (29)$$

To get the total current, the above equation is summed over all the members while considering the switches' role:

$$I_{tot}(\omega) = -j\omega d_{31} Y_p h_{pc} b \sum_{i=1}^{n} \left(P_i \sum_{m=1}^{\infty} \left\{ \eta_m(\omega) \left[W_m'(l) - W_m'(0) \right] \right\} \right) - j\omega \frac{\varepsilon_{33}^s b l}{h_p} V(\omega) \sum_{i=1}^{n} P_i^2 \quad (30)$$

The parameter P_i^2 would always be equal to 1. The voltage across the load is its impedance times the current; $V(\omega) = Z(\omega) I_{tot}(\omega)$. This leads to the second key equation needed:

$$V(\omega) \left[\frac{1}{Z(\omega)} + j\omega \frac{\varepsilon_{33}^s b l n}{h_p} \right] = j\omega \sum_{m=1}^{\infty} \kappa_m \eta_m(\omega) \quad (31)$$

Equations (26) and (31) can be combined to give the voltage output, $V(\omega)$, as a function of base acceleration, $a(\omega)$. Substituting for $\eta_m(\omega)$ from Equation (26) into Equation (31) gives:

$$V(\omega) \left[\frac{1}{Z(\omega)} + j\omega \frac{\varepsilon_{33}^s b l n}{h_p} \right] = j\omega \sum_{m=1}^{\infty} \kappa_m \left(\frac{-\kappa_m V(\omega) + \gamma_m a(\omega)}{\omega_m^2 - \omega^2} \right) \quad (32)$$

The term $c_0 = \frac{\varepsilon_{33}^s b l n}{h_p}$ is the capacitance of the transducer at low frequency. Considering the battery being connected to the resistive load, the impedance can be approximated by a capacitor, parallel with a resistor. Therefore, total load admittance would be: $\frac{1}{Z(\omega)} = c_b j\omega + \frac{1}{R}$. The resistance of the load is represented by R and c_b denotes the capacitance of the battery. The damping is modeled as modal damping by adding the term $2\zeta\omega_m j\omega$ to $\omega_m^2 - \omega^2$.

The Key Transfer Functions

Rearrangement of Equation (32) results in the following transfer function:

$$V(\omega)=\frac{\sum_{m=1}^{\infty}\frac{\gamma_m\kappa_m}{\omega_m^2+2\zeta\omega_m j\omega-\omega^2}}{\frac{1}{Rj\omega}+c_{bat}+c_0+\sum_{m=1}^{\infty}\frac{\kappa_m^2}{\omega_m^2+2\zeta\omega_m j\omega-\omega^2}}a(\omega) \quad (33)$$

The power output of the energy harvester can be calculated from:

$$\frac{p_{rms}(\omega)}{a^2(\omega)}=\frac{V^2(\omega)}{2Ra^2(\omega)}=\frac{1}{2R}\left(\frac{\sum_{m=1}^{\infty}\frac{\gamma_m\kappa_m}{\omega_m^2+2\zeta\omega_m j\omega-\omega^2}}{\frac{1}{Rj\omega}+c_{bat}+c_0+\sum_{m=1}^{\infty}\frac{\kappa_m^2}{\omega_m^2+2\zeta\omega_m j\omega-\omega^2}}\right)^2 \quad (34)$$

Equation (34) gives the rms output power at the specific frequency, ω. Since the power–voltage relation is not linear, we cannot use the fraction in Equation (34) as a transfer function.

Replacing for $V(\omega)$ from Equation (33) in Equation (23) gives the Fourier transforms of the modal functions $\eta_m(\omega)$:

$$\frac{\eta_m(\omega)}{a(\omega)}=\frac{-1}{\omega_m^2+2\zeta\omega_m j\omega-\omega^2}\times\left(\kappa_m\frac{\sum_{p=1}^{\infty}\frac{\gamma_p\kappa_p}{\omega_p^2+2\zeta\omega_p j\omega-\omega^2}}{\frac{1}{Rj\omega}+c_{bat}+c_0+\sum_{p=1}^{\infty}\frac{\kappa_p^2}{\omega_p^2+2\zeta\omega_p j\omega-\omega^2}}+\gamma_m\right) \quad (35)$$

The vibrations of the points on the structure can be calculated using Equations (5) and (35). As an example, the tip deflection Fourier transform can be obtained from the following:

$$\frac{w_{tip}(\omega)}{a(\omega)}=\sum_{m=1}^{\infty}\frac{-1}{\omega_m^2+2\zeta\omega_m j\omega-\omega^2}\times\left(\kappa_m\frac{\sum_{p=1}^{\infty}\frac{\gamma_p\kappa_p}{\omega_p^2+2\zeta\omega_p j\omega-\omega^2}}{\frac{1}{Rj\omega}+c_{bat}+c_0+\sum_{p=1}^{\infty}\frac{\kappa_p^2}{\omega_p^2+2\zeta\omega_p j\omega-\omega^2}}+\gamma_m\right)W_{mn}(x_{end}) \quad (36)$$

Arrangement of the Switches

As illustrated in Figure 2, the switches select between the direct and inverse connection of each of the members to the load. Since the members' vibrations can be in phase or out of phase with each other, the switches can be used to prevent cancellation of currents from different members. The state of each switch is determined based on the sign of the current produced by that member which in turn is a function of the mode shapes. Each mode shape, therefore, prescribes the switches' states in a certain manner. Since the peak power outputs occur at resonances, we can determine the switches states based on the mode which is dominantly excited by the base vibrations. Using Equation (28), the current due to electromechanical coupling, when member i is excited close to the mth natural frequency, is:

$$i_{mi}=-d_{31}Y_p h_{pc} b\dot{T}_m\left[W_{mi}^{'}(l)-W_{mi}^{'}(0)\right] \quad (37)$$

If the mth mode is dominantly vibrating, the states of the switches are assigned as follows to make all the currents passing through different members have identical signs:

$$P_i=Sign\left(W_{mi}^{'}(l)-W_{mi}^{'}(0)\right);\quad m:\text{mode number},\ i:\text{member number} \quad (38)$$

In most of the practical applications, the ambient oscillation frequency is close to the fundamental resonance. Moreover, the fundamental mode shape produces the most power; therefore, it is recommended to tune the switches according to the first mode shape.

RESULTS

We consider a practical zigzag structure for energy-harvesting application. The thickness of the piezoelectric layer on the MEMS energy harvesters is typically below 2 μm. We, therefore, set the thickness of the piezoelectric layer to 2 μm. The dimensions and material properties of the considered design (except the number of elements) are listed in Table 1. In all the case studies, the switches are set to optimize the power from the first mode. The number of parameters will be specified in each individual case study.

General Power Transfer Function

The power transfer function (Equation (34)) of a five-member zigzag structure is plotted in Figure 3. The harvested power peaks at the resonance frequency and varies with the load resistance.

The natural frequency of the structure changes from short circuit to open circuit frequency as the load resistance increases. The short circuit and open circuit natural frequencies are very close to each other. This means that the electromechanical coupling in the system is small. Comparing the thickness of the piezoelectric

Table 1. The specifications of the beams.

Length of the lateral beams, l (μm)	3000
Width of each of the beams, b (μm)	300
Center-to-center lateral distance of two adjacent beams, d (μm)	345
Thickness of the piezo layer, h_p (μm)	2
Thickness of the substructure, h_s (μm)	48
Tip mass (mg) (unless specified)	20.4
Link mass (μg)	40.8
Young's modulus of the piezo layer, Y_p (GPa)	66
Young's modulus of the substructure, Y_s (GPa; Ohashi et al., 1997)	140
Modulus of rigidity of the piezo layer, G_p (GPa)	25
Modulus of rigidity of the substructure, G_s (GPa)	38
Density of the piezo layer, ρ_p (kg/m^3)	7800
Density if the substructure, ρ_s (kg/m^3; Ohashi et al., 1997)	4400
Piezoelectric constant, d_{31} (pm/V)	−190
Permittivity, ε_{33}^s (nF/m)	15.93
Yield stress of the piezoelectric material (MPa; Fett et al., 1999)	40

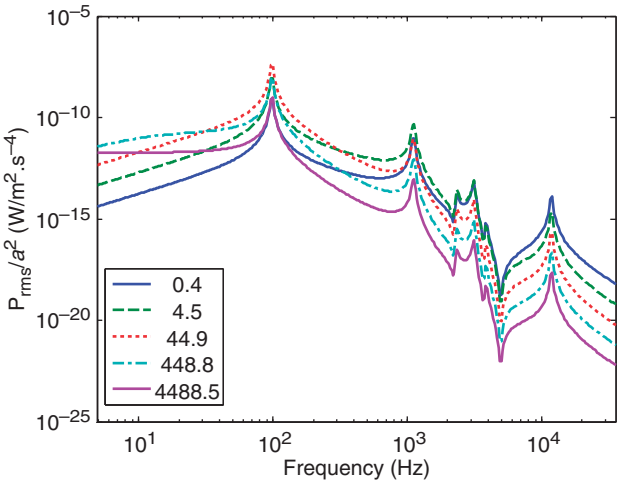

Figure 3. *The power transfer function of a five member zigzag structure; the legend is R (kΩ).*

layer (2 μm) with the thickness of the substrate (48 μm) justifies the small electromechanical coupling.

The harvested power peaks at the natural frequencies of the structure. However, Figure 3 reveals that the power produced at the fundamental frequency is significantly superior to the power at the higher natural frequencies. There are two reasons for this superiority. First, the connections in Figure 2 have been optimized for the first mode, and therefore, there is some power cancellation at the higher modes. The second reason is that the higher modes are less excited by base translations. This comes from the fact that the modal parameter γ_m corresponding to the first mode is much larger than γ_m of the higher modes.

The Relation Between the Number of Members and the Harvested Power

The merit of the meandering design is demonstrated by considering a single-beam harvester, turning it to a zigzag shape by adding more and more beams of the same dimensions. The power harvested from 13 meandering designs has been illustrated in Figure 4. The designs share the beam dimensions (specified in Table 1), but they have different number of members. The number of members in each design is noted at the peak of its power transfer function.

It can be seen that adding the number of members increases the maximum power only to some extent. Quantitatively speaking, the maximum power increases by 2.5 times as we go from a single-beam to a nine-member meandering structure. Adding the number of members will no more increase the power output. The justification for this fact is that increasing the number of members makes the vibrations more and more torsional. A meandering structure with high number of beams has more piezoelectric material and can potentially harvest more power. But, since there is not as much bending deformation in the structure as in the few-member structures, the power it produces barely exceeds the power from few (less than 9) member structures.

What matters for power production, though, is not how much power is produced at the structures' natural frequency, but how much power is produced at the ambient excitation frequency. As can be seen in Figure 4, a design with more members has a significantly less fundamental frequency than a few-member design. By adjusting the number of members, we can reduce the natural frequency and approximately match the ambient excitation frequency. As a case study, we calculate the power harvested from hypothetical 50-Hz ambient oscillations. The results in Figure 5 show that the optimal design is an 11-member meandering structure which has its fundamental frequency closest to 50 Hz. That 11-member structure produces four orders of magnitude more power compared to its single-member predecessor. This is a big improvement in power production coming mainly from frequency matching.

An alternate was to reduce the natural frequency of a beam harvester could be simply making it longer. That, of course, significantly reduces its strength. We calculate the static safety factor of the structure by calculating the force and moments in the zigzag structure due to its own weight. The results have been illustrated in Figure 6. The safety factor of the optimal 11-member design is about 6.7 which suggests that the structure can easily sustain the loads.

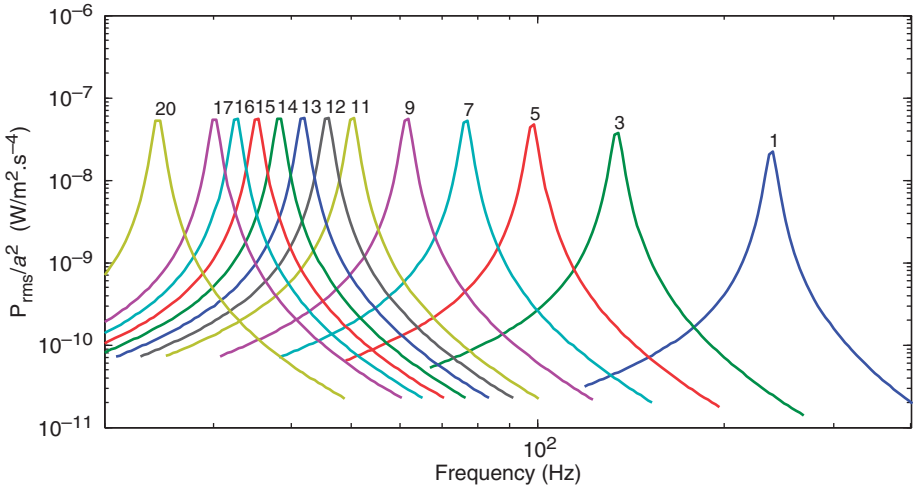

Figure 4. *Power transfer functions of different zigzag harvesters.*

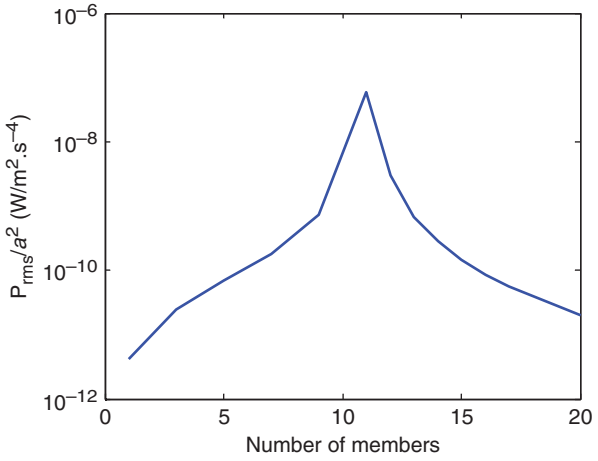

Figure 5. *The power harvested from 50-Hz ambient excitations.*

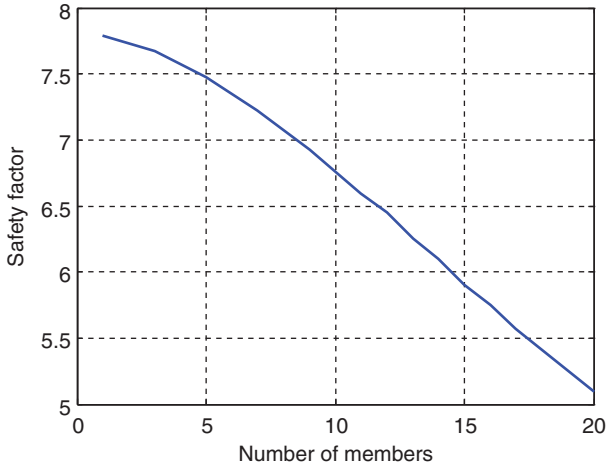

Figure 6. *The static safety factor.*

The Relation Between the Number of Beams and Mechanical Deflection

When the energy harvester is subjected to base acceleration it oscillates. In the design process, there should be enough offset between the zigzag structure and the base; otherwise, the structure will hit the base while vibrating. The offset is therefore determined by the vibration of the structure relative to the base. In the fundamental mode, the maximum deflection occurs at the tip of the meander. The figures in the subsection illustrate the outcome of Equation (36). Figure 7(a) illustrates that the relative tip acceleration transfer functions are almost identical for zigzag structures with different numbers of beams. Equivalently, Figure 7(b) shows that the tip displacement significantly increases with the number of beams. This is expected since the more-member structures have lower natural frequency. So, having the same acceleration implies that the displacement amplitude should be higher to compensate for the low frequency. The design implication of this result is that the gap between the zigzag structure and the base should be substantial for numerous-member zigzags. This may require etching of the wafer from the back in the micro-machining process. The presented model is based on the assumption that the deflection of the structure is small compared to the length of the beams. The validity of this assumption can be tested using Figure 7(b). If the deflection of each beam (not the tip deflection) is more than 10% of l, the geometric non-linearities become significant. In that case, non-linear modeling of vibration (Nayfeh and Mook, 1995) is required.

Another case study is calculation of tip vibrations of different structures subjected to a typical 50-Hz base excitation. As illustrated in Figure 8, the maximum displacement and acceleration both peak for an 11-member structure. The natural frequency of the 11-member structures is the closest match to the 50-Hz base excitation.

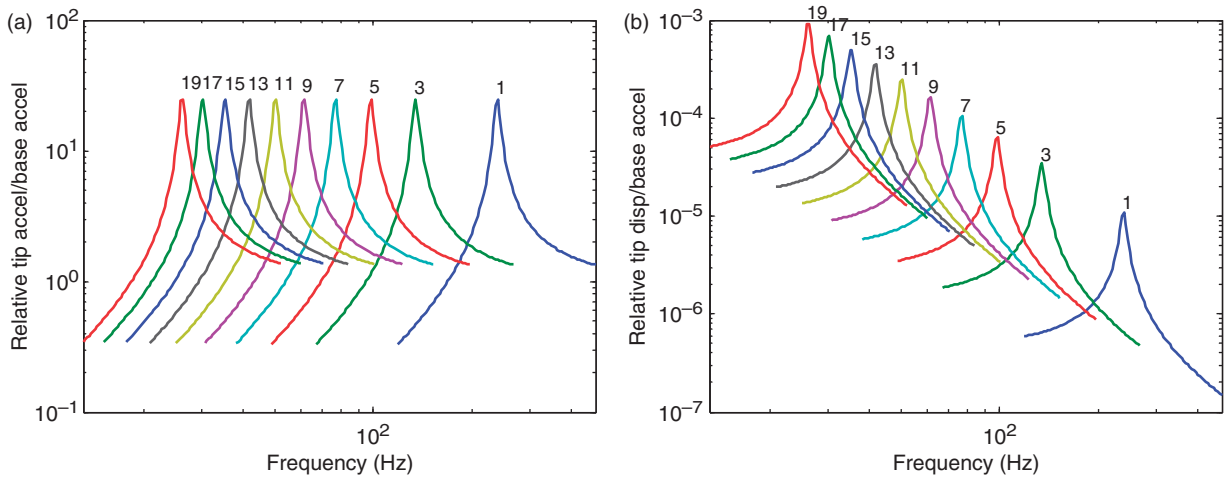

Figure 7. *Transfer functions of (a) relative tip acceleration and (b) relative tip displacement.*

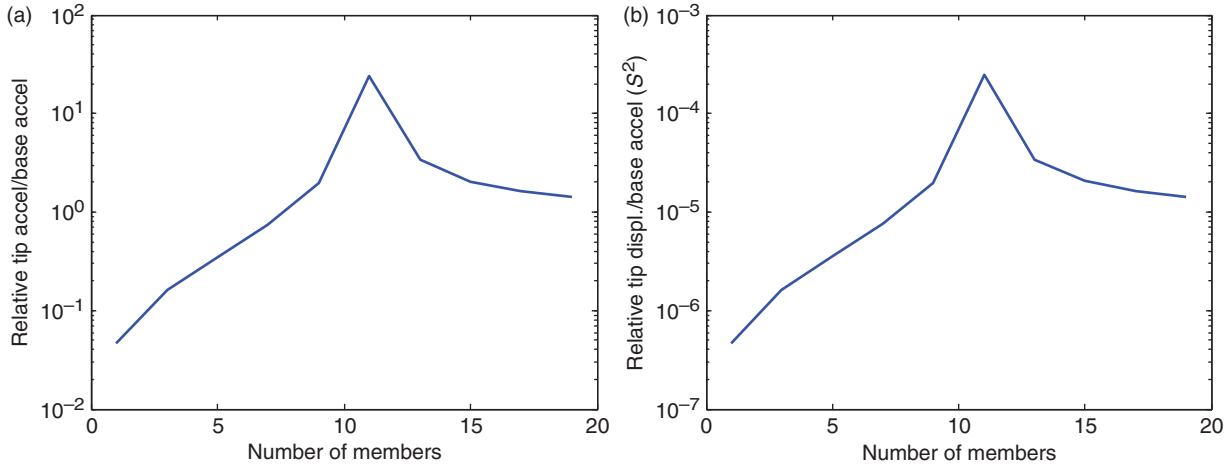

Figure 8. *Tip vibrations of meanders subject to 50-Hz base oscillations: (a) relative tip acceleration and (b) relative tip displacement.*

Relation Between the Load Resistance and Power Output

The power harvested by the zigzag MEMS harvester depends on the load resistance. As illustrated in Figure 9(a), the power peaks when the load resistance is about 67 kΩ. The electromechanical coupling is negligible for the harvesting device and the short circuit and open circuit natural frequencies are indistinguishable. This causes the power to peak only at a certain frequency and at a specific resistance. If the coupling in the harvester was larger, the optimal resistance for the short circuit frequency would be different from the optimal load for the open circuit frequency.

Optimized Design: the Thickness Determines the Number of Elements

We now go a step further and optimize the number of elements, the tip mass, and the load and focus on the power production from structures with different thicknesses. As discussed earlier in this section, the thickness of the piezoelectric layer is limited to about 2 μm. The substrate thickness, however, can be freely selected. The thicker the substrate is the larger the fundamental frequency of a single beam; however, we can do the frequency matching by appropriately selecting the number of members in the zigzag design. In this section, we also tune the tip mass such that the static safety factor of the structure is always 3.

Figure 10(a) illustrates that if we choose a thicker substrate, we need to use a more-member structure to match the excitations frequency. However, this pays off and the harvester power of a thicker structure will be higher. Figure 10(b) shows the tip mass ratio (mass of the tip mass/mass of one beam) that give a safety factor of 3. It can be seen that the thicker the substrate, the larger the tip mass can be. This translates to larger γ_m and correspondingly more power. Therefore, although

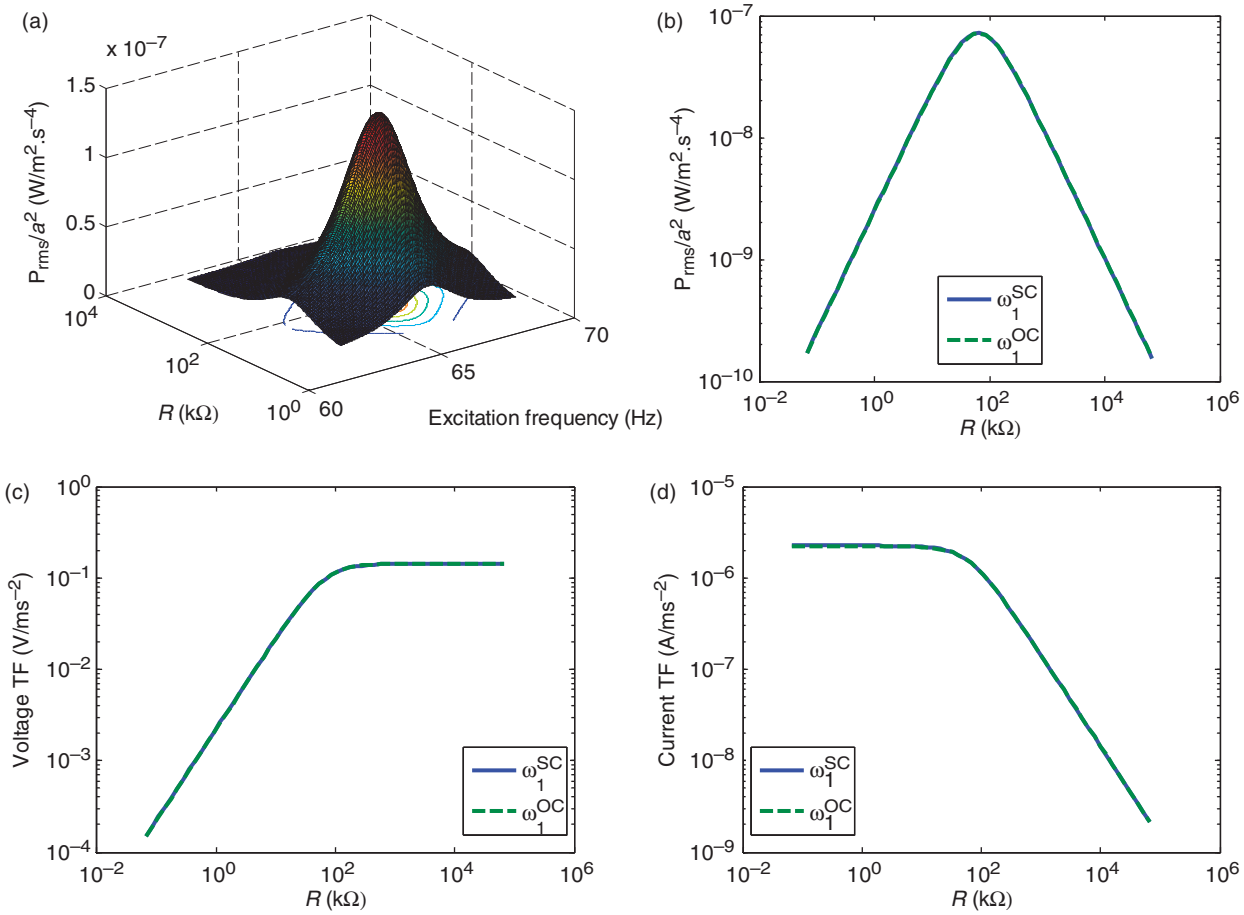

Figure 9. *The effect of load resistance on ((a) and (b)) power output from harvester, (c) voltage output, and (d) current output of the meander.*

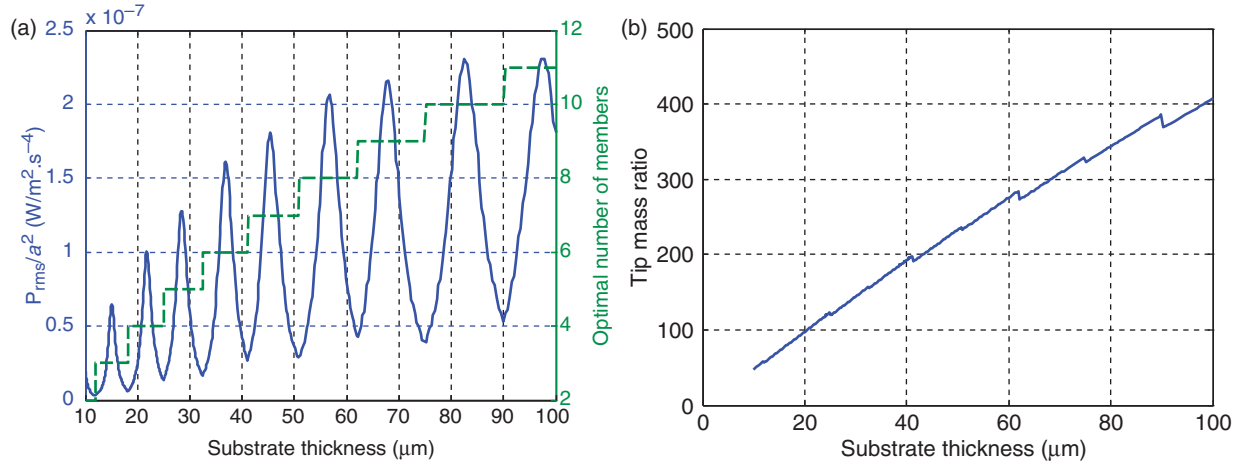

Figure 10. *Optimized design: (a) number of members and power output and (b) tip mass ratio.*

the thickness of the piezoelectric layer is unchanged, the thicker beams produce more power. Figure 10(a) once more demonstrates the importance of frequency matching. The fact that we only have integer values for number of beams means that the frequency matching cannot be perfectly done. The perfect frequency matching happens for some thicknesses, while some others will be slightly off resonance. That is the reason for the oscillatory variation of power with the thickness changes.

CONCLUSION

The electromechanical vibration of the micro-scale zigzag structure for energy harvesting was modeled. The model utilizes the previous derivation of natural frequencies and mode shapes. Using the modal analysis approach, a multi-mode coupled model was derived. The power output of the structure as well as the deflection of the structure was exactly modeled. A connection scheme was developed to minimize power cancellation by proper connection of electrical outlets of individual beams. As a case study, a micro-zigzag structure was considered. It was shown that by tuning the natural frequency of the structure, the meandering design can increase the power output by four orders of magnitude. The relation between the number of members and the power output was presented. In addition, the mechanical vibrations of zigzag structures with various numbers of members and the effect of electrical load on the power output were elaborated. Finally, it was shown that if the number of members and the electric load is fully optimized, the thicker the substrate, more the power can be harvested.

ACKNOWLEDGMENT

This study was performed under the support of the US Department of Commerce, National Institute of Standards and Technology, Technology Innovation Program, Cooperative Agreement Number "70NANB9H9007."

This study was supported in part by the Institute for Critical Technology and Applied Science (ICTAS).

REFERENCES

Anton, S. and Sodano, H. 2007. "A Review of Power Harvesting using Piezoelectric Materials (2003–2006)," *Smart Materials and Structures*, 16:1.

Arnold, D. 2007. "Review of Microscale Magnetic Power Generation,' *IEEE Transactions on Magnetics*," 43:3940–3951.

Beeby, S.P., Tudor, M.J. and White, N.M. 2006. "Energy Harvesting Vibration Sources for Microsystems Applications," *Measurement Science and Technology*, 17:175.

Blevins, R. 1979. "Straight Beams," *Book, Straight Beams*, Krieger, Malabar, Florida, p. 190.

Booker, J. and Kitipornchai, S. 1971. "Torsion of Multilayered Rectangular Section," *Journal of the Engineering Mechanics Division*, 97:1451–1468.

Cook-Chennault, K., Thambi, N. and Sastry, A. 2008. "Powering MEMS Portable Devices—A Review of Non-regenerative and Regenerative Power Supply Systems with Special Emphasis on Piezoelectric Energy Harvesting Systems," *Smart Materials and Structures*, 17:043001.

Erturk, A. and Inman, D. 2008. "A Distributed Parameter Electromechanical Model for Cantilevered Piezoelectric Energy Harvesters," *Journal of Vibration and Acoustics*, 130:041002.

Fang, H., Liu, J., Xu, Z., Dong, L., Wang, L., Chen, D., Cai, B. and Liu, Y. 2006. "Fabrication and Performance of MEMS-based Piezoelectric Power Generator for Vibration Energy Harvesting," *Microelectronics Journal*, 37:1280–1284.

Fett, T., Munz, D. and Thun, G. 1999. "Tensile and Bending Strength of Piezoelectric Ceramics," *Journal of Materials Science Letters*, 18:1899–1902.

Hu, H., Xue, H. and Hu, Y. 2007. "A Spiral-Shaped Harvester with an Improved Harvesting Element and an Adaptive Storage Circuit," *Ultrasonics, Ferroelectrics and Frequency Control, IEEE Transactions on*, 54:1177–1187.

Jeon, Y., Sood, R., Jeong, J. and Kim, S. 2005. "MEMS Power Generator with Transverse Mode Thin Film PZT," *Sensors & Actuators: A. Physical*, 122:16–22.

Karami, M.A. and Inman, D.J. 2011. "Analytical Modeling and Experimental Verification of the Vibrations of the Zigzag Micro-Structure for Energy Harvesting," *Journal of Vibration and Acoustics*, 133:011002.

Karami, M.A., Yardimoglu, B. and Inman, D.J. 2010. "Coupled Out of Plane Vibrations of Spiral Beams for Micro-scale Applications," *Journal of Sound and Vibration*, 329:5584–5599.

Kuehne, I., Marinkovic, D., Eckstein, G. and Seidel, H. 2008. "A New Approach for MEMS Power Generation Based on A Piezoelectric Diaphragm," *Sensors & Actuators: A. Physical*, 142:292–297.

Leo, D.J. 2007. *Engineering Analysis of Smart Material Systems*, Wiley, Hoboken, New Jersey.

Liu, J.-Q., Fang, H.-B., Xu, Z.-Y., Mao, X.-H., Shen, X.-C., Chen, D., Liao, H. and Cai, B.-C. 2008. "A MEMS-based Piezoelectric Power Generator Array for Vibration Energy Harvesting," *Microelectronics Journal*, 39:802–806.

Lu, F., Lee, H. and Lim, S. 2004. "Modeling and Analysis of Micro piezoelectric Power Generators for Micro-electromechanical-systems Applications," *Smart Materials and Structures*, 13:57–63.

Nayfeh, A. and Mook, D. 1995. *Nonlinear Oscillations*, Wiley-VCH, Germany.

Ohashi, M., Nakamura, K., Hirao, K., Toriyama, M. and Kanzaki, S. 1997. "Factors Affecting Mechanical Properties of Silicon Oxynitride Ceramics," *Ceramics International*, 23:27–37.

Priya, S. 2007. "Advances in Energy Harvesting using Low Profile Piezoelectric Transducers," *Journal of Electroceramics*, 19:167–184.

Priya, S. and Inman, D. 2008. *Energy Harvesting Technologies*, Springer, NY.

Shen, D., Park, J., Ajitsaria, J., Choe, S., Wikle, H. and Kim, D. 2008. "The Design, Fabrication and Evaluation of a MEMS PZT Cantilever with an Integrated Si Proof Mass for Vibration Energy Harvesting," *Journal of Micromechanics and Microengineering*, 18:55017.

Zheng, Q. and Xu, Y. 2008. "Asymmetric Air-spaced Cantilevers for Vibration Energy Harvesting," *Smart Materials and Structures*, 17:055009.